Fatigue life modelling of railway prestressed concrete sleepers

Li, Dan; Kaewunruen, Sakdirat; You, Ruilin; Liu, Ping

DOI:
10.1016/j.istruc.2022.05.053

Fatigue life modelling of railway prestressed concrete sleepers

Dan Li[1,2], Sakdirat Kaewunruen[1,2*], Ruilin You[3], Ping Liu[4]

[1] Department of Civil Engineering, School of Engineering, University of Birmingham, Birmingham B15 2TT, United Kingdom

[2] TOFU Lab (Track engineering and Operations for Future Uncertainties), School of Engineering, University of Birmingham, Birmingham B15 2TT, United Kingdom

[3] Railway Engineering Institute, China Academy of Railway Sciences, Beijing 100081, China

[4] Department of Civil Engineering, Jiangsu University of Science and Technology, Zhenjiang 215002, China

*** Correspondence:**
Sakdirat Kaewunruen
S.Kaewunruen@bham.ac.uk

Abstract

The railway sleepers, which transfer wheel loads to the formation, are an important component of railway track systems. Prestressed concrete is the most commonly used type of railway sleeper around world. Crushing is a common problem on concrete sleepers, which include excessive flexural, shear, and bond stresses. The most causes of crushing in prestressed concrete sleepers are dynamic loads. However, accumulated damage due to cyclic loads can also cause crushing. Much previous research has investigated the impact load characteristics and the ultimate load capacity of prestressed concrete railway sleepers. There is a gap in the knowledge in fatigue failure for prestressed concrete sleepers. This study presents new results of extensive numerical and analytical investigations aimed at predicting fatigue lives under cyclic loads. A numerical study validated by 30 full-scale experimental tests is executed to assess fatigue performance, while theoretical fatigue analysis methods based on S-N curve and Miner linear cumulative damage are introduced for benchmarking. This paper presents a remaining fatigue life assessment for prestressed concrete sleepers and contrasts with the theoretical results. Parametric studies discuss the effect of support conditions, dynamic load distribution, and track stiffnesses on prestressed concrete sleepers. This paper highlights the rationales associated with the development of fatigue limit state. The outcome of this paper will provide design flexibility and improve railway sleeper maintenance and inspection criteria.

Keywords: prestressed concrete sleeper, fatigue, cyclic load, finite element method (FEM), numerical analysis

1 Introduction

Railway transportation provides safe, economical, and comfortable transport for either passengers or goods [1, 2]. An important component of railway systems are railway sleepers. The main functions of railway sleepers are distributing axle loads from rails to the substructures of railway systems and holding the rails at the proper gauge [1, 3]. Prestressed concrete railway sleeper is the most commonly used type of sleeper around world with its economic cost, long service life, and sound structural performance. However, prestressed concrete sleepers can still be damaged due to flexural, shear, or bond stresses. In long-term service, fatigue load heavily influences progressive cracking. Fatigue failure can be defined as structural failure below the stress limit under cyclic loading [4]. A worldwide survey of most critical concrete sleeper failures was conducted by W. Ferdous, A. Manalo (2014), and the results indicated fatigue is one of the top 5 most critical causes of failure for concrete sleepers [5]. Fatigue failure can be defined as a failure happens below the stress limit of a material when it has been applied to repeated loads. In concrete sleepers, crushing or cracking under compressive stress can be considered ordinarily as the failure criterion to define fatigue state in design process. A global trend that the increases in traffic flow and train tonnage cause accumulated damage due to cyclic loads, which might cause railway sleeper failure in long-term service life.

The permissible stress or allowable stress design concept for prestressed concrete sleepers is used in many countries [6]. This method is based on the permissible stress of materials and a load factor is used to increase the static axle load to incorporate dynamic effects [7]. However, the permissible stress method may underestimate the material strength, while dynamic loads are not considered thoroughly. A concept based on a probabilistic model of the load resistance, limit state method, is developed for railway sleepers. It applies the magnitude of factors may be varied so that they may be used either with the plastic conditions in the ultimate state or with the more elastic stress range at working loads [8]. Ultimate limit state is the railway sleepers must be able to withstand the loads against failure. Fatigue limit state is a concrete sleeper services under cyclic loading for years and the accumulated damage progressively reaches failure [9].

Previous research by Wakui, H and Okuda, H (1997) found cracking of concrete sleepers developed rapidly due to repeated impact loads, and it was suggested a fatigue limit state should be included in concrete sleeper design [10]. Many experimental and analytical investigations regarding dynamic behaviour of prestressed concrete railway sleepers have been conducted by Kaewunruen, S and Remennikov, A.M, (2007, 2014, 2013) and their research provides amount of data for analysis of cyclic loads and fatigue damage [11-13]. The fatigue loading tests were carried out by Rantala et al (2018) to analyse the fatigue properties of the sleepers and the effect of fatigue on their stiffness [14]. Šimonová et al presented a study on the influence of the age and level of concrete fatigue on prestressed railway sleeper [15]. Maekawa, K. et al (2006) conducted the 3D fatigue analysis which predicts the fatigue life of reinforced concrete slabs [16]. Zhang, C. et al (2019) developed 3D concrete T-shape girder in order to investigate the fatigue performance of the carriageway plates of bridge [17]. These studies provide a fundamental understanding of fatigue behaviour in concrete structures.

In this research, it is possible to better understand the fatigue life of the railway sleepers associated with various service conditions. On this ground, there is clearly a need to carry out an investigation of the fatigue life simulation. This article presents a numerical simulation of the fatigue life of prestressed concrete sleepers. Finite element analysis was conducted to investigate the life cycle of prestressed concrete sleepers. Chinese Type III prestressed concrete sleepers were used to study fatigue life. A physical model of the sleeper is established and validated. The results show the effect of typical support conditions, various impact loads, and different track stiffnesses on service life of the prestressed concrete sleeper. A theoretical fatigue life assessment method is also introduced in order to validate the numerical model. The findings presented in this study aim to develop a fatigue life assessment model, which will eventually help railway engineers to better estimate the service life of railway sleepers under various conditions.

2 Fatigue life assessment method

2.1 Damage accumulation method

Previous research has presented the fatigue life assessment method of concrete sleepers [9, 18]. The theoretical assessment method is based on the damage accumulation method and extending Miner's rule, and can be used to evaluate the fatigue life under constant amplitude cyclic loads. For each cyclic load, the critical tensile stress of the prestressing tendons of the prestressed concrete sleeper can be calculated and the fatigue life for the cyclic load can be determined. The cumulative damage index is given by:

$$\sum D_i = \sum_i \frac{n(\Delta\sigma_i)}{N(\Delta\sigma_i)} \quad (1)$$

where $n(\Delta\sigma_i)$ is the applied number of cycles at a stress range $\Delta\sigma_i$; $N(\Delta\sigma_i)$ is the resisting number of cycles at a stress range $\Delta\sigma_i$.

The S-N curve is the relationship between the magnitude of an alternating stress and the number of cycles until there is failure for a selected material. The maximum applied number of cycles at an alternating stress can be determined and it is expressed as failure cycles (fatigue life) [19, 20]. The S-N curve for prestressing steel is shown in **Figure 1** and the failure cycles of prestressing steel under cyclic loads can be estimated by:

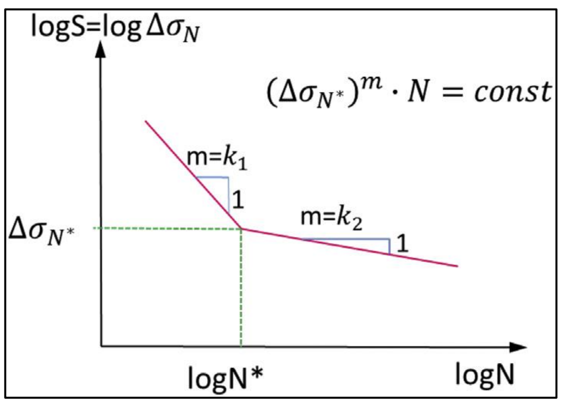

Figure 1. S-N curve for prestressing steel [19]

If $(\Delta\sigma > \Delta\sigma_{N^*})$

$$\log N_f = \log N^* - k_1[\log(\Delta\sigma) - \log(\Delta\sigma_{N^*})] \quad (2)$$

If $(\Delta\sigma < \Delta\sigma_{N^*})$

$$\log N_f = \log N^* + k_2[\log(\Delta\sigma_{N^*}) - \log(\Delta\sigma)] \quad (3)$$

where $\Delta\sigma$ is the stress range of the prestressing tendons; $\Delta\sigma_{N^*}$ is the stress range at N^* cycles; k_1, k_2 are the stress exponents. **Table 1** illustrates parameters of prestressing steel S-N curve. (Note: this S-N curve is able to define the type of prestressing tendons used in this research)

S-N curve of prestressing steel used for	**Stress exponent**			$\Delta\sigma_{N^*}$ **at** N^* **cycles (Mpa)**
	N^*	k_1	k_2	

Pre-tensioning	10^6	5	9	185

Table 1. Parameters of S-N curve for prestressing steel [19]

2.2 Fatigue life assessment

To assess fatigue life, the cracking progression of the railway sleeper needs to be analysed. In the initial stage, no cracking appears and the concrete stress at the bottom fibre can be calculated by:

$$\sigma_{cF}^{b} = \frac{nA_{ps}\sigma_{se}}{A_t} + \frac{nA_{ps}\sigma_{se}e}{I_t}y_t \tag{4}$$

where σ_{se} is the effective stress per prestressing tendon; A_{ps} is the cross-section area of a tendon; e is the eccentricity; n is the number of tendons; A_t is the transformed area of the sleeper; I_t is the inertia moment of transformed section before cracking; y_t is the distance of the centroidal axis of transformed area from soffit.

The cracking moment is calculated by:

$$M_{cr} = I_t\frac{\sigma_{cF}^{b} + f_{cf}}{y_t} \tag{5}$$

where f_{cf} is the tensile strength of the sleeper.

As the cracking progresses, the neutral axis of the sleeper cross-section will change. Therefore, the distance y_{CG} from the centre gravity of the effective transformed area to the top of the compressed area needs to be determined by:

$$y_{CG} = root\left[\left[S_{pcII} - n_eA'_{p3}\left(h - y_{cg} - d_3\right) - n_eA'_{p2}\left(h - y_{cg} - d_2\right) - n_eA'_{p1}\left(h - y_{cg} - d_1\right)\right], y_{cg}\right] \tag{6}$$

where the S_{pcII} is the first moment at the bottom fibre after cracking; A'_{pi} is the total area of the prestressing tendons at layer i; d_i is the distance from the prestressed tendons at layer i to the bottom of tension area; n_e is the modular ratio.

The effective transformed section can be estimated using the transformed area of sleeper cross-section A_{tII}:

$$A_{tII} = A_{cII} + n_eA_p \tag{7}$$

where A_{cII} is the effective concrete area of sleeper cross-section.

The moment of inertia of the cracking section is given by:

$$I_{cr} = I_{ccr} + n_eA'_{p3}\left(h - y_{cg} - d_3\right)^2 + n_eA'_{p2}\left(h - y_{cg} - d_2\right)^2 + n_eA'_{p1}\left(h - y_{cg} - d_1\right)^2 \tag{8}$$

where I_{ccr} is the inertia moment of effective centroid. (Note: the selected prestressed concrete sleeper has three layers of prestressing tendons, the equation (6)-(8) can be also applied for other cross-section of prestressed concrete sleepers.)

The effective inertia moment in the lifetime is calculated by:

$$I_{ef} = I_{cr} + (I_t - I_{cr})\left(\frac{M_{cr}}{M_{max}}\right)^3 \quad (9)$$

where I_t is the inertia moment of transformed section before cracking; M_{cr} is the cracking moment; M_{max} is the maximum bending moment at the section under cyclic loads.

$$\Delta\sigma_{pt1} = n_e \frac{M_{max} - M_{min}}{I_{ef}} \left(h - y_{cg} - d_1\right) \quad (10)$$

where M_{min} is the minimum bending moment at the section under cyclic loads.

Using the output value of $\Delta\sigma_{pt1}$, the failure cycles of the prestressing tendons under constant cyclic loading can be estimated by Equation (2) or (3).

3 Fatigue life simulation method

3.1 Fatigue analysis type in finite element method

In this study, ANSYS Workbench has been used to investigate the fatigue life of prestressed concrete sleepers. The aim of fatigue analysis in this simulation is to ascertain capability of a material to survive from the cyclic loads during service life. In general, fatigue analysis can be categorised into Strain Life, Stress Life, and Fracture Mechanics. The Strain Life method focuses on crack initiation where the strain can be directly measured. This method deals with relatively low cycles (less than 10^5 cycles). Fracture Mechanics is used to determine crack growth. The time from crack initiation to the crack growing to a critical size can be calculated using this method. Sometimes, Fracture Mechanics (crack growth) is used with the Strain Life method (crack initiation) to determine total fatigue life.

In this research, the Stress Life method is adopted. This method is typically characterised by an empirical S-N curve as part of material definition of the sleeper model and modified by a variety of factors dealing with relatively high cycles (more than 10^5 cycles). It should be noted that fatigue life results using the stress life method show the available life for the given fatigue analysis without considering crack propagation or fracture. Therefore, the output results represent the cycles until the sleeper will fail due to fatigue [21, 22].

3.2 Cyclic loading type

The Constant amplitude, Proportional loading is applied in this research shown in **Figure 2**. Loading is of constant amplitude because only one set of FE stress results along with a loading ratio is required to calculate the alternating and mean values. Loading is proportional since only one set of FE results are needed (principal stress axes do not change over time). Common types of constant amplitude loading are fully reversed (apply a load, then apply an equal and opposite load; a load ratio of –1) and zero-based (apply a load then remove it; a load ratio of 0). Since loading is proportional, looking at a single set of FE results can identify critical fatigue locations. Likewise, since there are only two loadings, no cycle counting or cumulative damage calculations need to be done [21, 22].

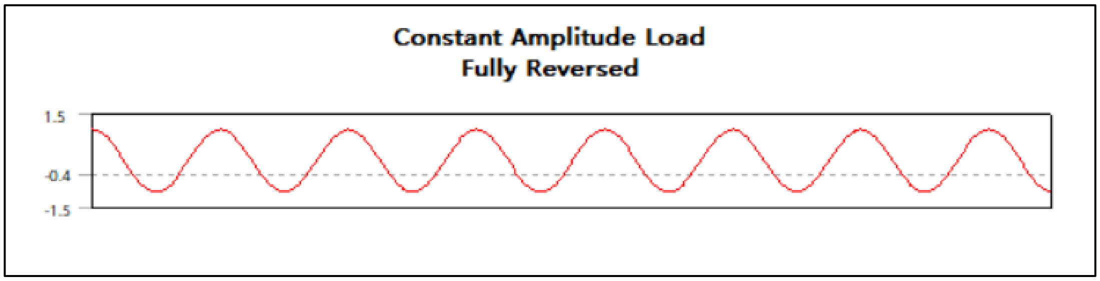

Figure 2. Constant amplitude load

3.3 Equivalent alternating stress

In analysis of fatigue using the Stress Life method, the S-N curve is required to relate the fatigue to the stress state. Therefore, the equivalent alternating stress is used to query the S-N curve to determine the fatigue life. The equivalent alternating stress is the stress used to query the fatigue S-N curve after accounting for fatigue loading type, mean stress effects, multiaxial effects, and any other factors in fatigue analysis. The equivalent alternating stress can be determined as following steps:

1. Calculate the alternating mean stress tensor.
2. Collapse alternating and mean stress from tensor to scalar using selected stress component.
3. Calculate the Equivalent Alternating Stress using the desired empirical stress theory, as specified by the Mean Stress Theory property of the Fatigue Tool object.

Several empirical options can be selected including Gerber, Goodman, and Soderberg theories as shown below. According to these theories, the value reported as the equivalent alternating stress is used to query the fatigue life from the S-N curve. The equivalent alternating stress is the last calculated quantity before determining the fatigue life [21, 22].

Gerber Equation:

$$\frac{\sigma_{Alternating}}{S_{Endurance\ Limit}} + \left(\frac{\sigma_{Mean}}{S_{Ultimate\ Strength}}\right)^2 = 1 \qquad (11)$$

Goodman Equation:

$$\frac{\sigma_{Alternating}}{S_{Endurance\ Limit}} + \frac{\sigma_{Mean}}{S_{Ultimate\ Strength}} = 1 \qquad (12)$$

Soderberg Equation:

$$\frac{\sigma_{Alternating}}{S_{Endurance\ Limit}} + \frac{\sigma_{Mean}}{S_{Yield\ Strength}} = 1 \qquad (13)$$

3.4 Fatigue life results

The simulation results of fatigue life are represented the number of cycles until the railway sleeper fails due to fatigue. In a Stress Life analysis with constant amplitude, if the equivalent alternating stress is lower than the lowest alternating stress defined in the S-N curve, the life at that point will be used [21, 22].

4 Prestressed concrete sleeper details

Chinese Type III prestressed concrete sleeper is used to study fatigue life. Material properties and section details are indicated in **Figure 3** and **Table 2** with the following parameters:

(1) Track gauge: 1435mm
(2) Concrete strength: C60
(3) Prestressing tendons: 10No. of 7mm dia. (tendon area: 384mm^2)
(4) Prestressing force: 420kN (pre-tensioning)

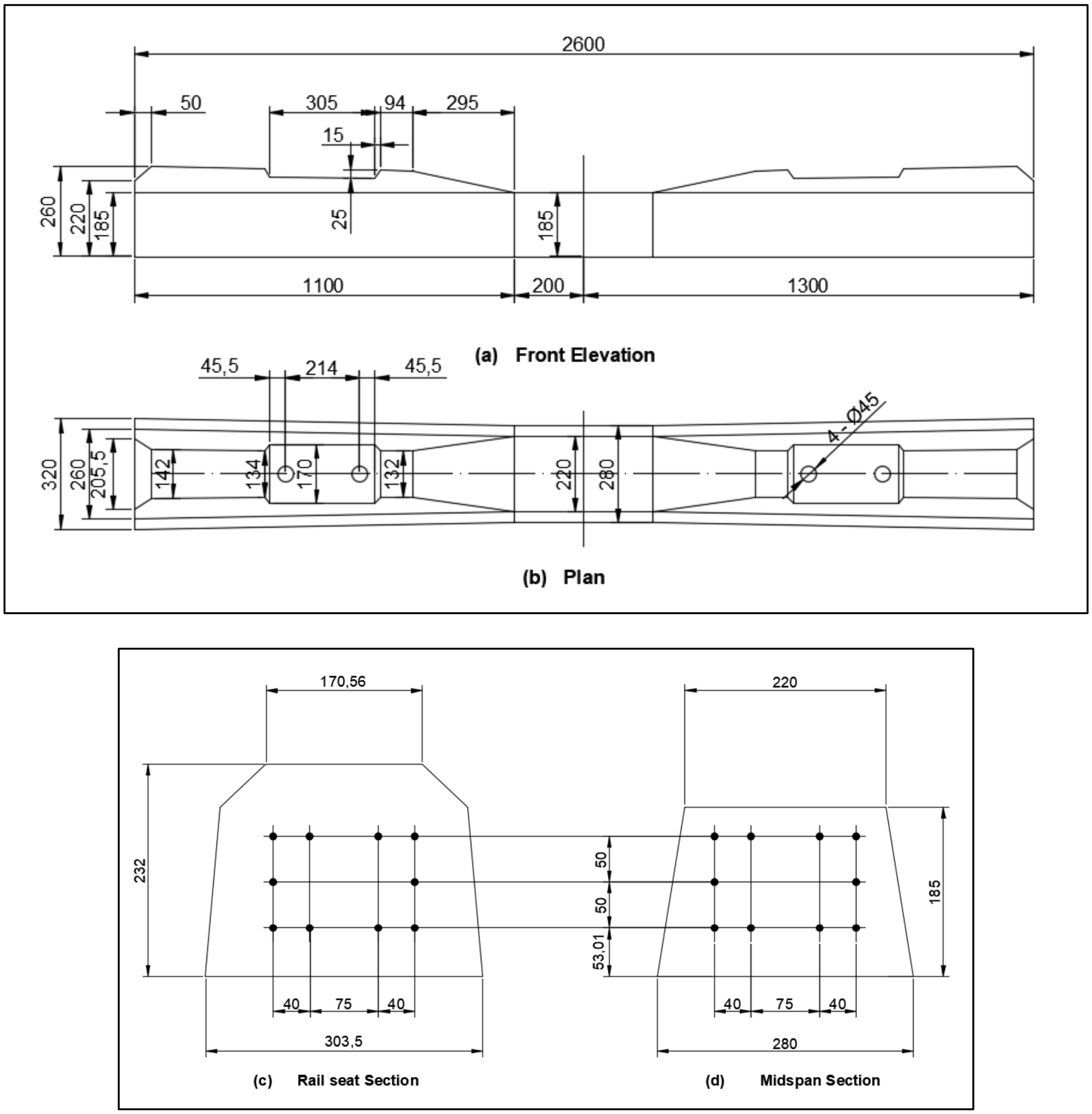

Figure 3. Chinese Type III prestressed concrete sleeper geometric details

Material properties	Basic variables	Value
Concrete	Mean compressive strength	65MPa
	Modulus of elasticity	33GPa
Prestressed wire	Yield strength	1570MPa

Modulus of elasticity	200GPa

Table 2. Material properties

5 Finite element model of the prestressed concrete sleeper

The finite element model was developed to study fatigue life. The sleeper model used in this study is made up of 3D solid elements shown in **Figure 4**. The finite element model is composed of railway sleeper, prestressed tendons, and ballast. The concrete of sleeper is modelled as solid elements with most of these elements being 10-node tetrahedron elements, while the prestressed tendons are modelled as beam elements. The ballast is also modelled as solid elements. The material constitutive model of the FE sleeper model follows the experimental data presented in Section 5.1. It should be noted that the S-N curve used for prestressing tendons of the sleeper model is assumed in terms of **Table 1**.

The engineering properties used in the FE modelling are illustrated in **Table 3**. These properties were selected because they were identical to a particular type of concrete sleeper manufactured in China. In the model, concrete, prestressing tendons, and ballast (block support) are considered to be well adhere. The No-Separation contact type is used to simulate the constraints between concrete and prestressing tendons, which the bond slip and bursting are not considered. The contact type between the sleeper and ballast is Rough, which there is no sliding allowed. The bottom interface of tensionless ballast is set as fixed support and edges of ballast layer are set as free. The remaining boundary conditions at both rail seats have been set as hinges where the longitudinal and lateral displacements are restrained. In the simulation of prestressing force transfer, the Thermal Condition is used to define the temperature in the tendons, which the thermal load can be regarded as the prestressing force. After the prestressing force transferred, the cyclic load can be applied to the FE sleeper model for analysing fatigue life of the prestressed concrete sleeper. It should be noted that the size of ballast model is 3200mm×900mm×300mm, which the selection follows the sleeper density with 1308 sleepers per km. The thickness of ballast layer is usually 250mm to 300mm, thus the 300mm thickness of ballast is accepted.

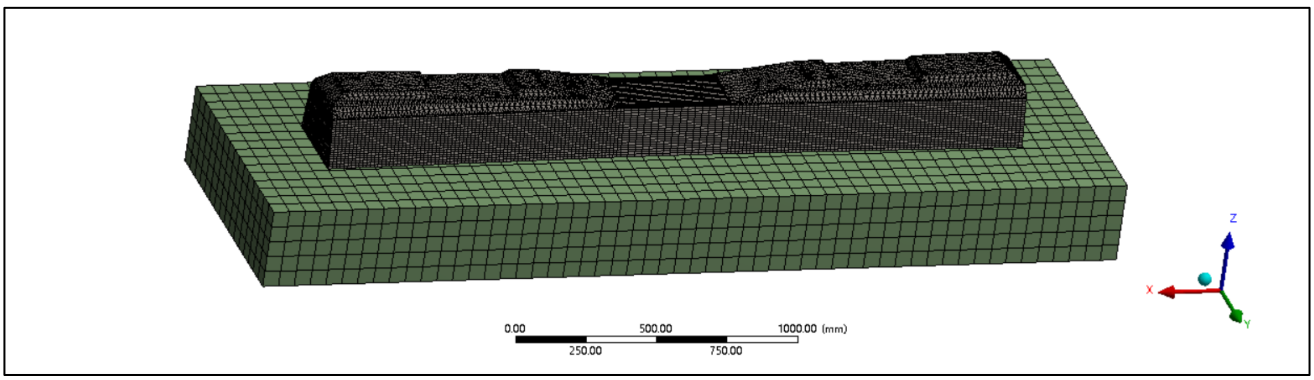

Figure 4. Finite element model of the Chinese Type III prestressed concrete sleeper

Parts	Modulus of elasticity (MPa)	Density (kg/m^3)	Poisson's ratio
Sleeper	33000	2400	0.23
Ballast	1500	1800	0.20
Tendons	200000	9800	0.30

Table 3. Material properties used in the FE model

5.1 Model validation

To validate the model, the static capacity test of Chinese Type III prestressed concrete sleeper is used to verify structural and material properties of the FE sleeper model [23, 24]. An experimental programme as conducted at Beijing Jiaotong University (apparatus shown in **Figure 5**) used to validate the FE sleeper model. In the experiment, the loading jack was applied to a rubber plate located just above the surface of the centre of the sleeper. The loading level increases up to 140kN. The DIC (digital imagine correlation) was selected to obtain load-deflection response.

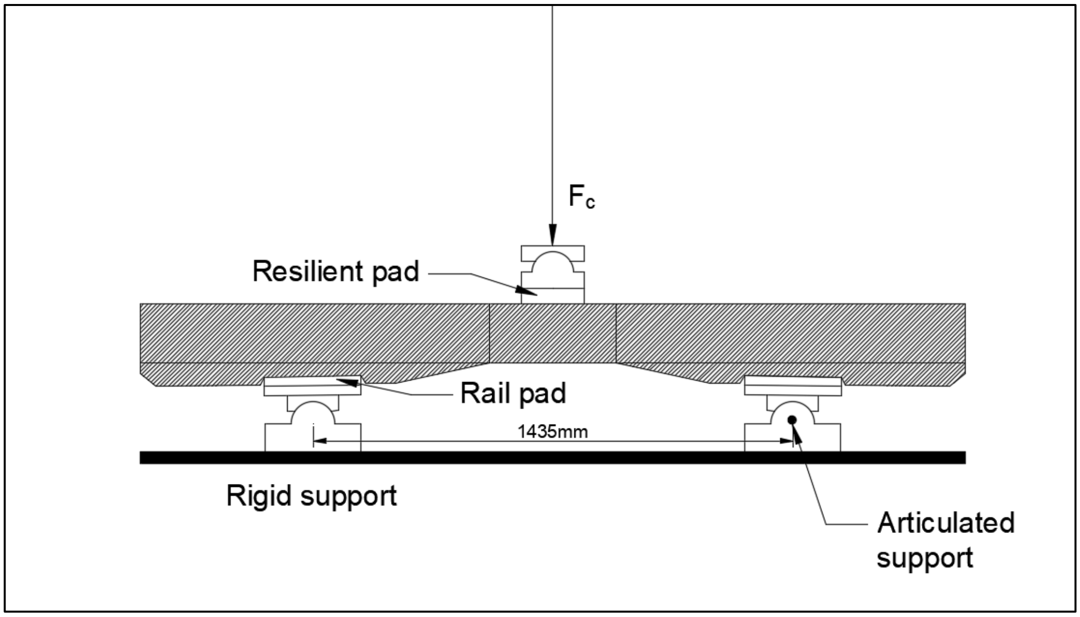

Figure 5. Apparatus of the static capacity test of sleeper

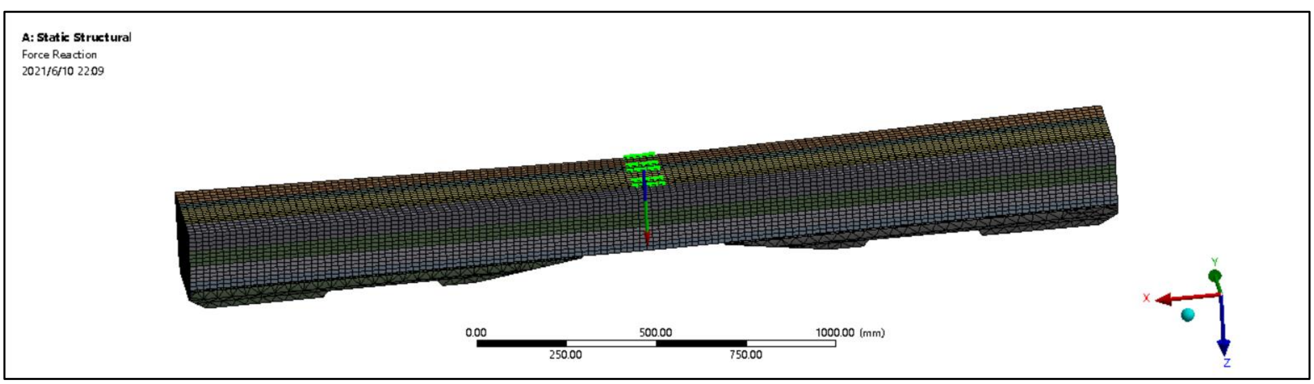

Figure 6. Static capacity test simulation for FE sleeper model validation

In order to validate the quality of the FE sleeper model, the numerical results have been compared with experimental results from the static capacity test in previous research [26]. **Figure 6** shows the static capacity simulation for FE sleeper model material and structural validation. **Figure 7** presents the comparison between the FE analysis and experimental results. The results are found to be in very good agreement with the static capacity test. The maximum difference between the experimental and numerical results is only 5.99%.

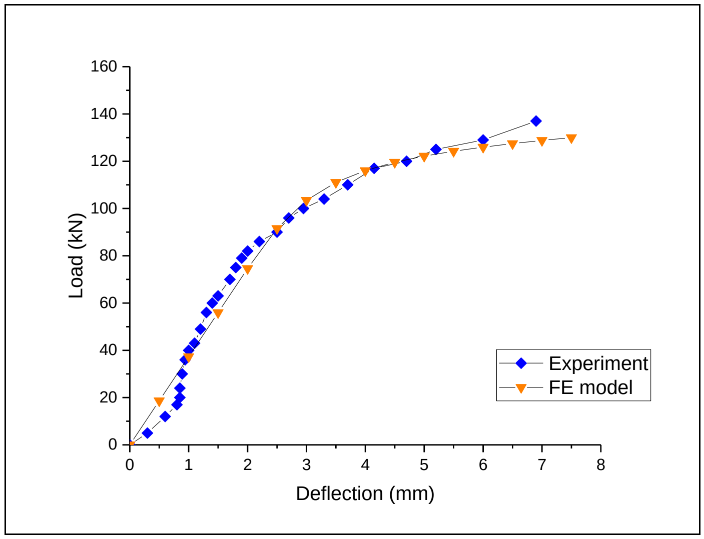

Figure 7. Load-deflection response between FE results and experimental results

6 Results of the fatigue life prediction

Section 2 introduces the theoretical fatigue life assessment method. The cyclic loads (dynamic loads) between 55kN to 365kN are chosen to calculate the fatigue life. Each dynamic load is assumed as constant which can calculate only one fatigue life for both numerical and theoretical assessment method. The output results represent the sleeper will fail under the constant dynamic load after output number of cycles. The simulation of fatigue life refers to the results of theoretical fatigue life assessment. **Figure 8** presents the cyclic loads setting. The pressure is applied at the rail seat area and the magnitude range of cyclic loads (dynamic loads) is following theoretical calculation in order to compare the results. The S-N curve used in predicting fatigue life is shown in **Table 1** of Section 2. The comparison of numerical and theoretical fatigue life results is demonstrated in **Table 4** and **Figure 9**. From **Table 4**, it can be seen that the errors between numerical and theoretical results range from 0.03% to 35.13%. The average error is 13.03%. From **Figure 9**, it is seen that the FE analysis results are quite similar to the theoretical fatigue life results. In order to validate the numerical fatigue model, the experimental data is also used to compare with numerical and theoretical results. Parvez and Foster have conducted fatigue experiments of prestressed concrete sleepers to observe failure cycles [25, 26]. Two specimens are chosen from fatigue experiments to calculate the average of the failure cycles presented in **Table 5**. Based on their test results, the comparison between experimental, theoretical, and numerical results is shown in **Table 6**. A good correlation between the numerical, theoretical, and experimental results provides a reliable method for further parametric study.

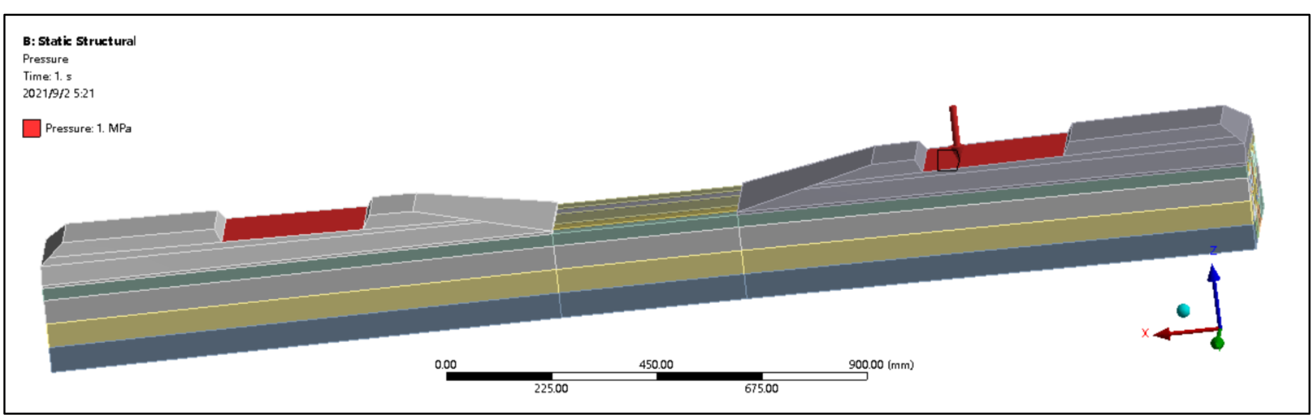

Figure 8. Setup for fatigue life simulation

Load (kN)	Life cycles (numerical)	Life cycles (theoretical)	Error %
55	3.47E+10	4.19E+10	20.59
65	1.54E+10	1.70E+10	10.31
75	7.71E+09	7.24E+09	6.19
85	3.43E+09	3.23E+09	5.95
95	1.68E+09	1.50E+09	10.80
105	8.79E+08	7.21E+08	17.94
120	3.76E+08	3.59E+08	4.39
130	1.73E+08	1.85E+08	6.70
140	8.48E+07	9.77E+08	15.14
150	4.38E+07	5.30E+07	20.95
160	2.39E+07	2.95E+07	23.41
175	1.41E+07	1.68E+07	18.75
185	8.62E+06	9.74E+06	13.03
195	5.41E+06	5.77E+06	6.66
205	3.48E+06	3.48E+06	0.03
215	2.30E+06	2.14E+06	6.92
225	1.76E+06	1.33E+06	24.21
245	1.21E+06	8.04E+05	33.36
260	8.49E+05	5.61E+05	33.89
270	6.79E+05	4.45E+05	34.45
280	5.48E+05	3.56E+05	35.13
290	3.44E+05	2.86E+05	16.92
305	2.34E+05	2.31E+05	1.30
315	1.88E+05	1.88E+05	0.09
325	1.52E+05	1.54E+05	1.00
335	1.23E+05	1.26E+05	2.76
345	1.00E+05	1.05E+05	4.37
355	85186	86773	1.86
365	72829	72364	0.64

Table 4. Comparison of theoretical and numerical fatigue life results

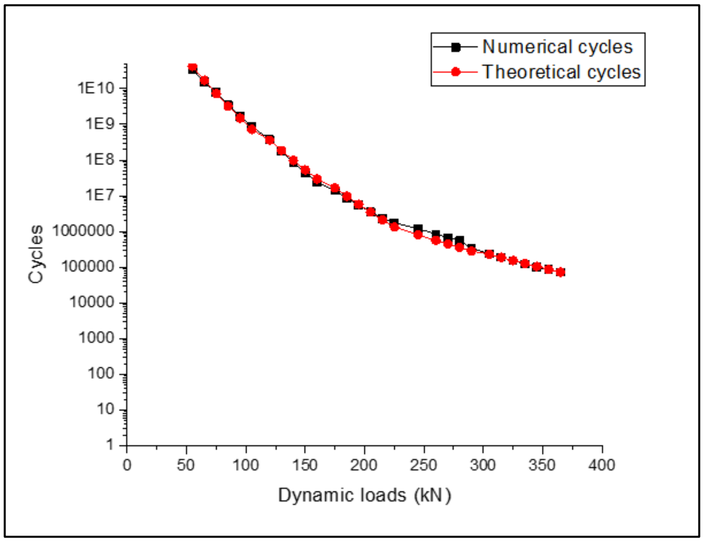

Figure 9. Comparison between numerical and theoretical fatigue life results

Specimen ID	Failure cycles	Average	Standard Deviation
SF2-a	773793	896290	173236
SF3-a	1018787		

Table 5. Experimental failure cycles [25]

Failure cycles				
Experimental result	Theoretical result	Deviation ratio %	Numerical result	Deviation ratio %
896290	889577	0.75	849000	5.28

Table 6. Comparison between experimental, theoretical, and numerical results

7 Parametric study

The comparison between the theoretical and model results implies that the fatigue life under various dynamic loads can be predicted and simulated use the FE model. Therefore, the validated FE model can be utilised to analyse the fatigue life under other critical conditions.

7.1 Support conditions

In a conventional track system, railway sleepers are usually laid on ballast and subgrade. It is usually assumed there is full contact between sleeper and ballast for analysis and design purposes. However, voids and hanging support conditions could occur and can cause problems to both sleeper and track system. Previous studies [27, 28] indicate 5 typical sleeper/ballast contact patterns used to analyse how fatigue life is affected by the support conditions. The sleeper/ballast contact patterns are illustrated in **Figure 10**. Full contact between sleepers and ballast is typically assumed for analysis and design purposes. The voids and pockets in the sleeper/ballast contact interface form between sleepers and the ballast underneath that could cause problems to both the sleepers and the track system as a whole. The selected support patterns are practical concerns in actual railway track problems. In the simulation, the positive reaction at rail-seat and the negative reaction at mid-span are considered and the fatigue life depends on the minimum of output. The ratio of the void length and sleeper length is controlled to observe the change of fatigue life under different support patterns. The simulation has been conducted for each pattern. Loads of between 55kN to 325kN are applied in the FE model.

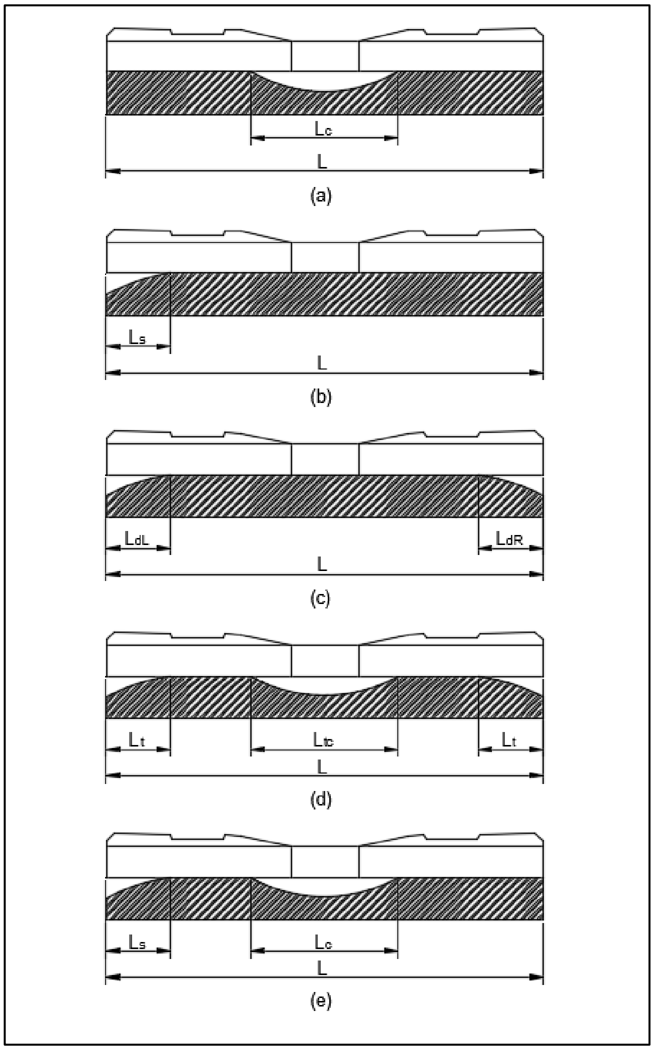

Figure 10. Sleeper/ballast contact patterns: (a) central void, (b) single hanging, (c) double hanging, (d) triple hanging, (e) side-central voids

7.1.1 Central void

The central void is a void which forms at the centre of the sleeper and expands symmetrically in both directions. The ratio of the central void length to the sleeper length is given:

$$\alpha_c = \frac{L_c}{L} \quad (11)$$

where L_c is the central void length; L is the sleeper length.

The ratio α_c of 30.77% (800/2600), 38.46% (1000/2600), 46.15% (1200/2600), 53.85% (1400/2600) were respectively simulated to analyse fatigue life. **Figure 11** shows the simulation setup and stress distribution contour. In the FE model, the length of central void area can be adjusted and expanded in both directions. **Figure 12** indicates the results of fatigue life in the central void support condition.

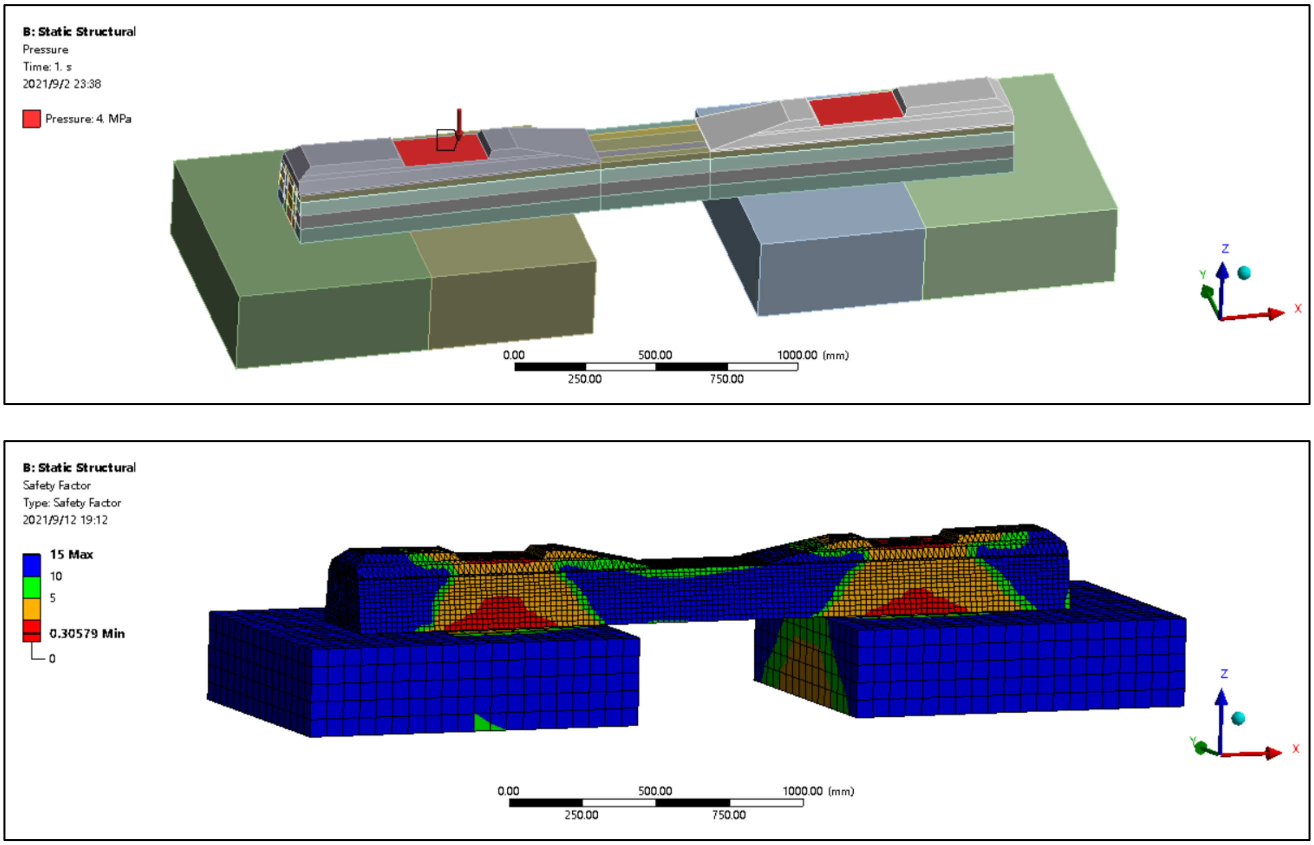

Figure 11. Simulation of the central void support condition

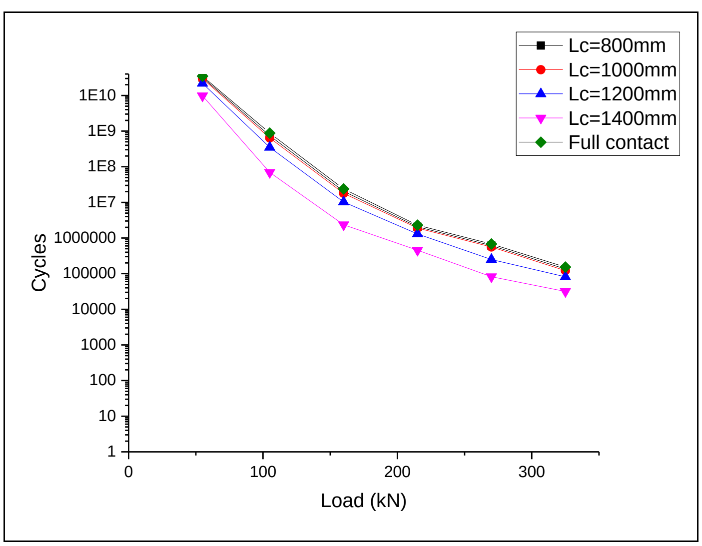

Figure 12. Comparison of the central void pattern results

Figure 11 shows the maximum stress occurs at bottom rail-seat area, which the minimum fatigue life should happen at rail-seat area. The effect of the central void on the fatigue life of the prestressed concrete sleeper is shown in **Figure 12**. The results show that central void length of less than 1000mm (ratio α_c less than 38.46%) is unlikely to influence the fatigue life in comparison with full contact pattern, while the change of fatigue life is just around 2%. The central void length increases to 1200mm (ratio α_c=46.15%), and the fatigue life falls by 51% on average for loads of between 55kN to 325kN. When the central void length increases to 1400mm (ratio α_c=53.85%), the fatigue life reduces by 83%. It is obvious that the fatigue life is insensitive when the small void ratios from 0 to 40% are used.

7.1.2 Single hanging

The single hanging is a void that forms at the one end of the sleeper and grows incrementally to the other end of the sleeper. The ratio of the single side void length to the sleeper length is given as:

$$\alpha_s = \frac{L_s}{L} \tag{12}$$

where L_s is the side void length; L is the sleeper length.

The ratio α_s of 11.54% (300/2600), 15.38% (400/2600), 19.23% (500/2600), 23.08% (600/2600) were respectively simulated to analyse the fatigue life. **Figure 13** shows the simulation setup and stress distribution contour. In the FE model, the length of the single side void area can be adjusted and expanded in the other direction. **Figure 14** indicates the results of fatigue life in the single hanging support condition.

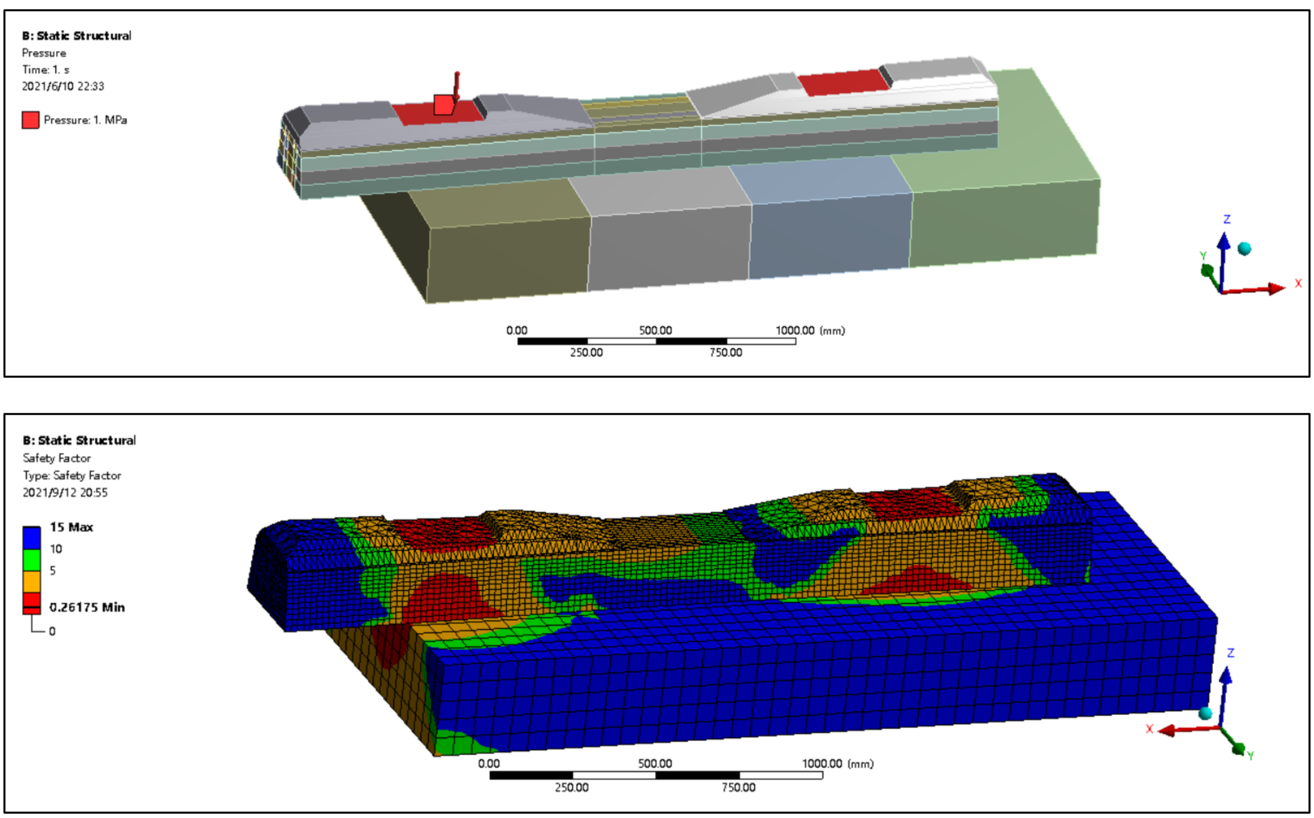

Figure 13. Simulation of the single hanging support condition

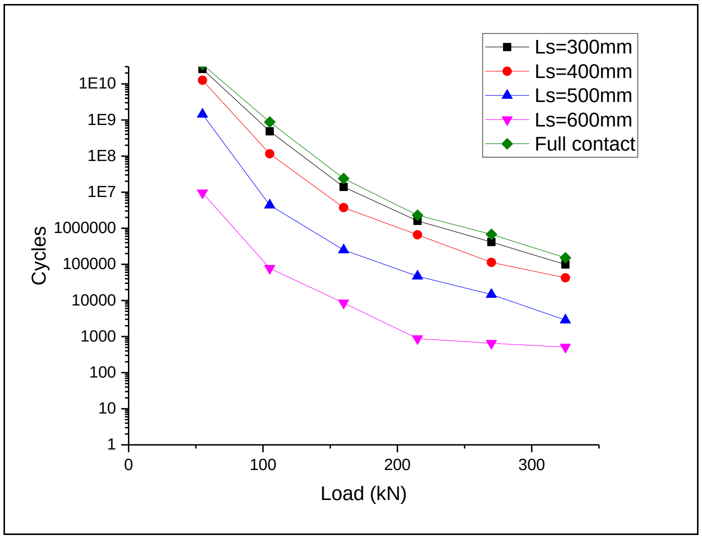

Figure 14. Comparison of the single hanging pattern results

Figure 13 shows the maximum stress occurs at bottom rail-seat area, which the minimum fatigue life should happen at rail-seat area. **Figure 14** presents the effect of the one end hanging condition on the fatigue life of the prestressed concrete sleeper. The fatigue life seems to be significantly affected by this support condition. Single hanging void lengths ranging from 300mm to 600mm are investigated. The fatigue life decreases when single hanging void length increases. When the side hanging length is 300mm (ratio α_s=11.54%), the fatigue life reduces by 35.98% in average. The difference between 400mm (ratio α_s=15.38%), 500mm (ratio α_s=19.23%) voids and the full contact pattern are 76.89% and 98.04% respectively. When the side hanging length increases to 600mm (ratio α_s=23.08%), the fatigue life reaches half of the full contact support pattern which is a 99.90% change.

7.1.3 Double hanging

The double hanging is when voids are present at both ends of the sleeper. The ratio of the double side void length to the sleeper length is given as:

$$\alpha_d = \frac{L_{dL}}{L}, \beta_d = \frac{L_{dR}}{L} \tag{13}$$

where L_{dR}, L_{dL} are the void length at right and left sides; L is the sleeper length.

The ratio α_d, $\beta_d$of 11.54% (300/2600), 15.38% (400/2600), 19.23% (500/2600), 23.08% (600/2600) are respectively simulated to analyse the fatigue life. **Figure 15** shows the simulation setup and stress distribution contour. In the FE model, the length of each side void area can be adjusted and expanded in each direction. The void length on both sides is assumed equal. **Figure 16** indicates the results of fatigue life in the double hanging support condition.

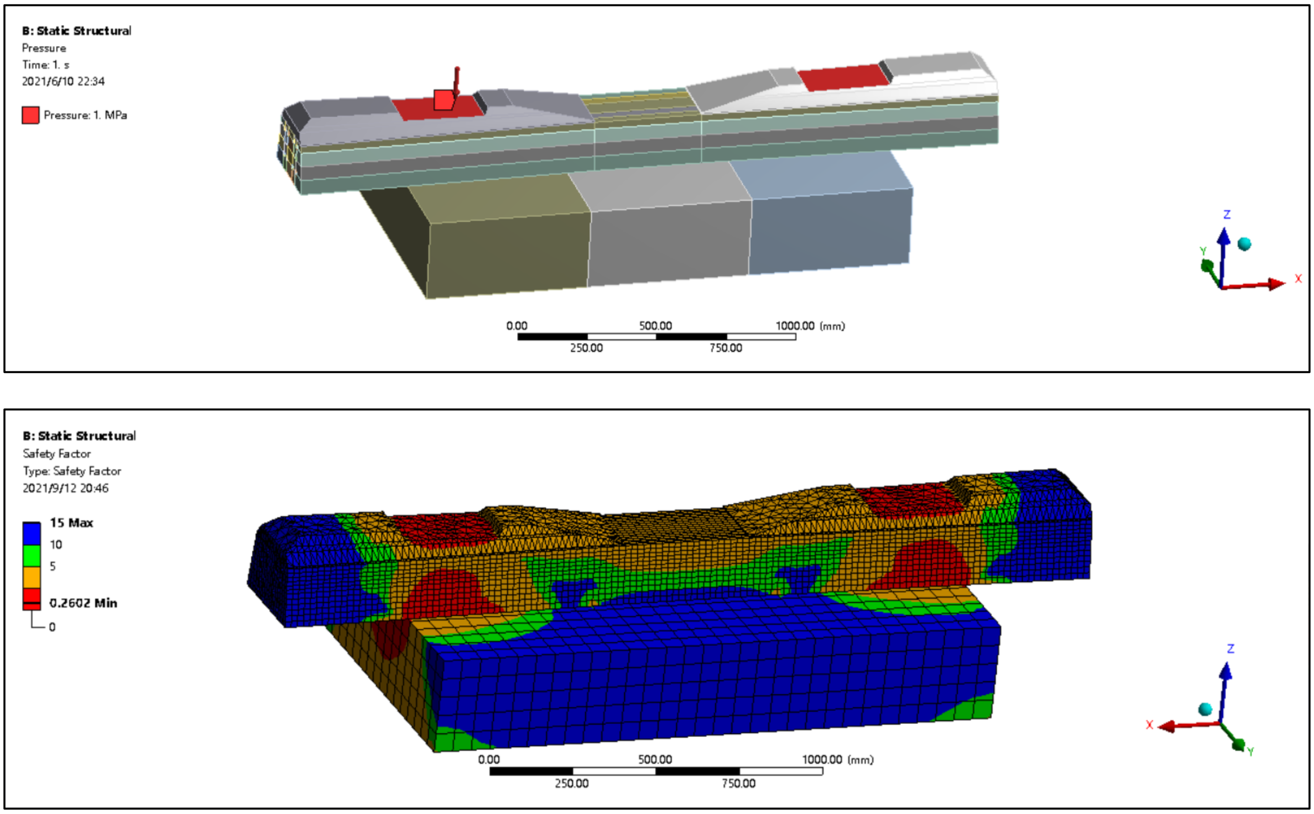

Figure 15. Simulation of the double hanging support condition

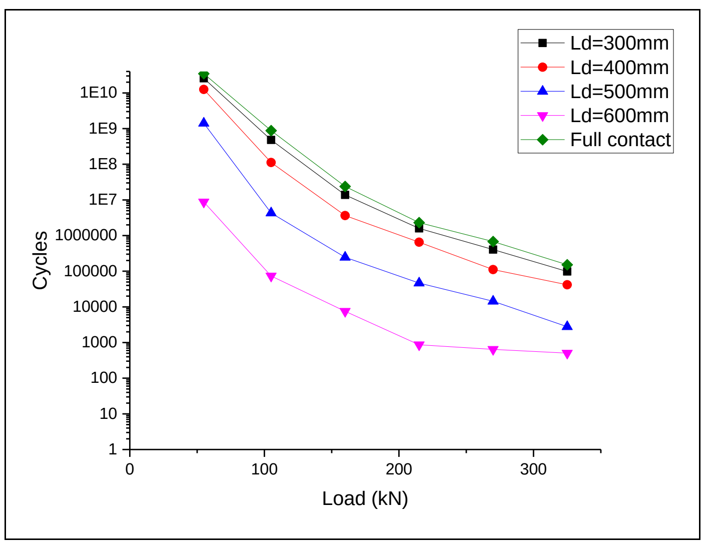

Figure 16. Comparison of the double hanging pattern results

Figure 15 shows the maximum stress occurs at bottom rail-seat area, which the minimum fatigue life should happen at rail-seat area. The changes in fatigue life of the prestressed concrete sleeper for varying lengths of double hanging voids are illustrated in **Figure 16**. The results are similar to the single hanging support pattern. Single hanging void lengths from 300mm to 600mm are investigated. The fatigue life decreases as single hanging void length increases. With the side hanging length at 300mm (ratio α_d=11.54%), the fatigue life reduces by 36.71% on average. When the side hanging length increases to 600mm (ratio α_d=23.08%), the fatigue life only reaches half of the full contact support pattern.

7.1.4 Triple hanging

The triple hanging is when there are voids at both ends and a pocket in the middle of the sleepers. The ratio of the triple side void length to the sleeper length is given as:

$$\alpha_t = \frac{L_t}{L}, \beta_t = \frac{L_{tc}}{L} \qquad (14)$$

where L_t is the void length at sides; L_{tc} is the void length at the centre; L is the sleeper length.

The ratio α_t, β_t of 11.54%/30.77% (300/2600; 800/2600), 19.23%/38.46% (500/2600; 1000/2600), 23.08%/30.77% (600/2600; 800/2600), 23.08%/46.15% (600/2600; 1200/2600) are respectively simulated to analyse the fatigue life. **Figure 17** shows the simulation setup and stress distribution contour. In the FE model, the length of each end void and centre void area can be adjusted and expanded. Only symmetrical cases are considered in this research. **Figure 18** indicates the results of fatigue life in the triple hanging support condition.

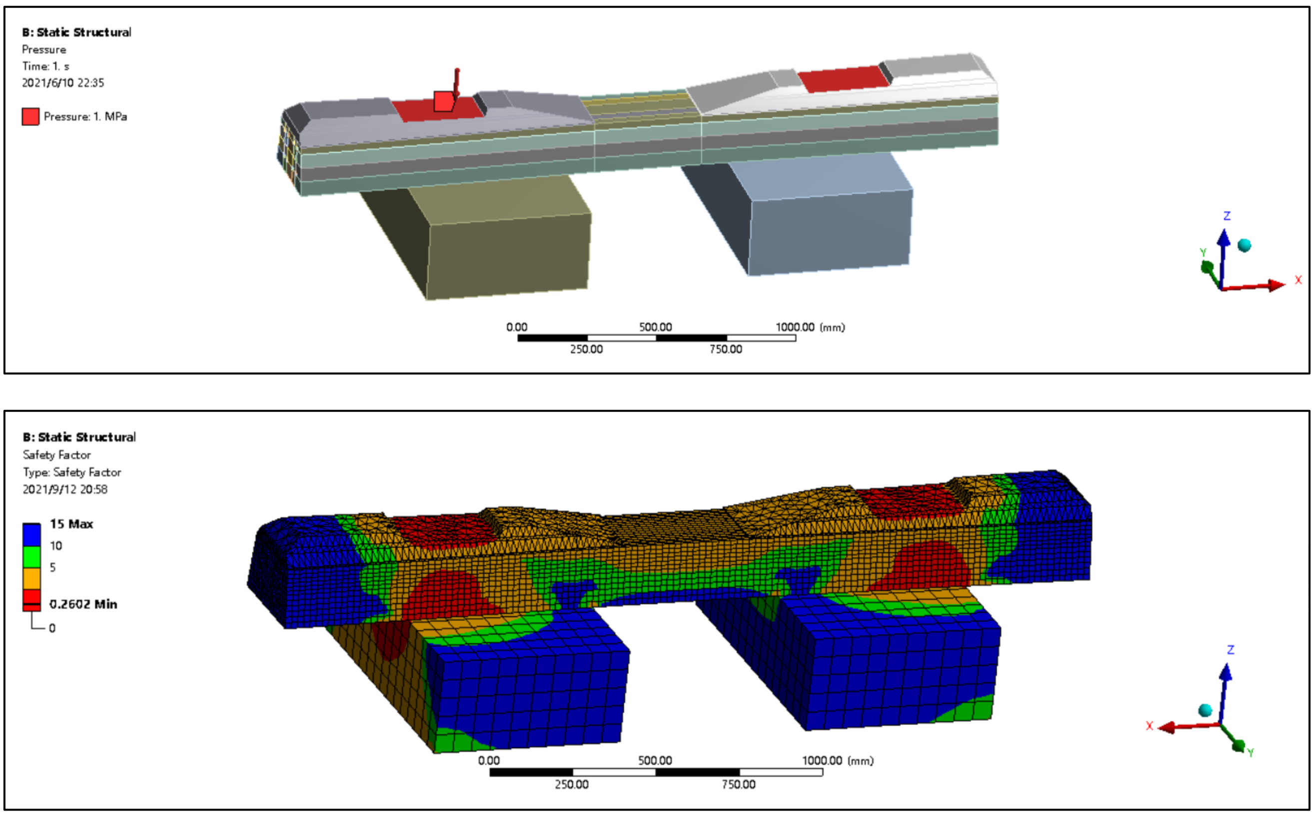

Figure 17. Simulation of triple hanging support condition

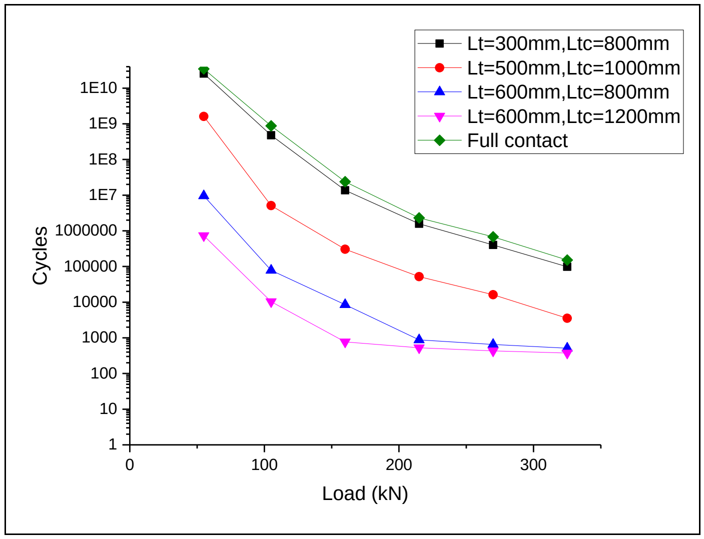

Figure 18. Comparison of the triple hanging pattern results

Figure 17 shows the maximum stress occurs at bottom rail-seat area, which the minimum fatigue life should happen at rail-seat area. The fatigue life of the voided prestressed concrete sleeper under triple void contact pattern is demonstrated in **Figure 18**. It is found that a small void ratio (α_t, β_t of 11.54%/30.77% (300mm/2600mm; 800mm/2600mm)) does not influence the fatigue life very much. In comparison with α_t, β_t of 19.23%/38.46% (500mm/2600mm; 1000mm/2600mm) and α_t, β_t of 23.08%/30.77% (600mm/2600mm; 800mm/2600mm), side voids have more sensitive effects than central voids. To observe the changes in large side hanging with different central voids, the α_t, β_t of 23.08%/30.77% (600mm/2600mm; 800mm/2600mm) and 23.08%/46.15% (600mm/2600mmm; 1200mm/2600mm) are investigated. At loads of between 55kN and 160kN, the large central voids of triple hanging support pattern have less fatigue life. However, when the large loads are applied (more than 215kN), the fatigue life becomes very similar to each other. This demonstrates that poor support conditions under large dynamic loads can easily result in failure on the prestressed concrete sleepers.

7.1.5 Side-central voids

The side-central voids are formed at the edge hanging and central void at the same time. The ratio of the side-central voids length to the sleeper length is given as:

$$\alpha_{s-c} = \frac{L_s}{L}, \beta_{s-c} = \frac{L_c}{L} \tag{15}$$

where L_{dR}, L_{dL} are the void length at right and left sides; L is the sleeper length.

The ratio α_{s-c} , β_{s-c} of 11.54%/30.77% (300/2600; 800/2600), 19.23%/38.46% (500/2600; 1000/2600), 23.08%/30.77% (600/2600; 800/2600), 23.08%/46.15% (600/2600; 1200/2600) are respectively simulated to analyse the fatigue life. **Figure 19** shows the simulation setup and stress distribution contour. In the FE model, the length of edge and central void area can be adjusted and expanded. The void length at both sides is assumed equal. **Figure 20** indicates the results of fatigue life in the side-central void support condition.

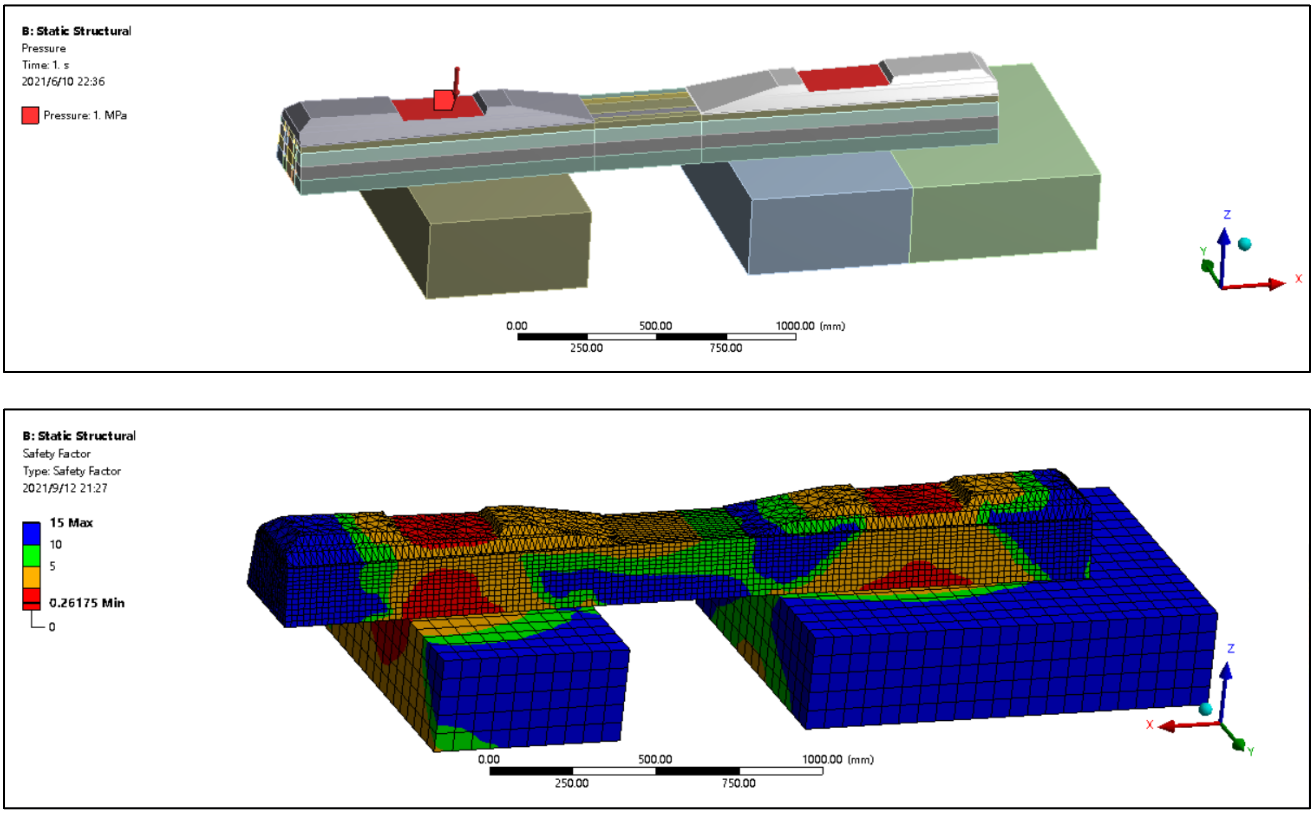

Figure 19. Simulation of side-central void support condition

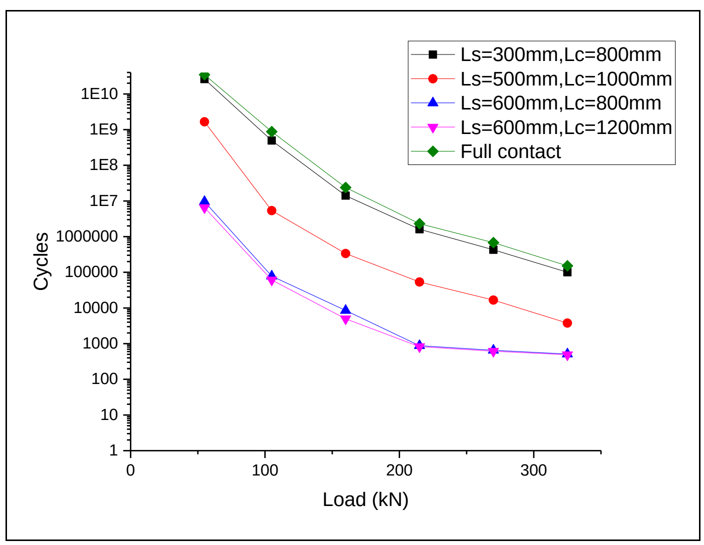

Figure 20. Comparison of the side-central void pattern results

Figure 19 shows the maximum stress occurs at bottom rail-seat area, which the minimum fatigue life should happen at rail-seat area. The changes in the fatigue life of the prestressed concrete sleepers due to side and central voids are illustrated in **Figure 20**. This contact pattern can be considered to be a combination of central void and single hanging. In this support pattern, small voids (α_{s-c}, β_{s-c} of 11.54%/30.77% (300mm/2600mm; 800mm/2600mm)) do not have much influence on the fatigue life with the change being just 35.14%. From **Figure 20**, it can be seen that the same side voids but different central voids (α_t, β_t of 23.08%/30.77% (600mm/2600mm; 800mm/2600mm) and 23.08%/46.15%

(600mm/2600mmm; 1200mm/2600mm)), the results of the fatigue lives are very similar. The results also demonstrate the side voids have more influence than central voids.

7.2 Impact load distribution

The FE model analyses the fatigue lives under various magnitude of dynamic loads. The output results of fatigue lives are under a constant dynamic load. In the field, the railway sleepers could experience a wide range of dynamic loads. This section analyses the fatigue life under different impact load distributions. In this section, the support condition is set as full contact pattern.

A comprehensive investigation of actual impact loads was conducted by Leong, J and Kaewunruen, S (2007, 2007) [7, 28]. The frequency of occurrence of impact loads per year has been recorded, as shown in **Figure 21**. Over 1 year, data were obtained from two Teknis Wheel Condition Monitoring stations located on different heavy-haul mineral lines in Australia. A total of nearly six million passing wheels were measured. A number of 1,609,712 passing wheels measured for a year from unit trains with 26 tons to 28 tons axle loads were used in fatigue life analysis. The analysis of field measurement indicates over 96% of wheels created impact loads less than 50kN. However, there were still more than 40,000 passing wheels higher than 140kN. From **Table 4** above, it can be seen that large loads can significantly cause a reduction of fatigue life. Therefore, the effect of impact load distribution needs to be studied. The impact load distribution data is applied in the FE model. MATLAB is used to generate an impact load distribution and inputted into the numerical model.

The dashed line shown in **Figure 21** demonstrates the impact load distribution. The slope of the dashed line controls the impact load magnitude range and volume of occurrence of impact loads (the total cycles need to be close to field measurement). In this section, two cases of the impact load distribution are investigated and the field measurement data is regarded as the control group. Case 1 is the range of impact load up to 410kN with low volume of occurrence. Case 2 shows the impact load range up to 240kN but low volume of occurrence. The impact load distribution of Case 1 and Case 2 are shown in **Figure 22** and **Table 7**.

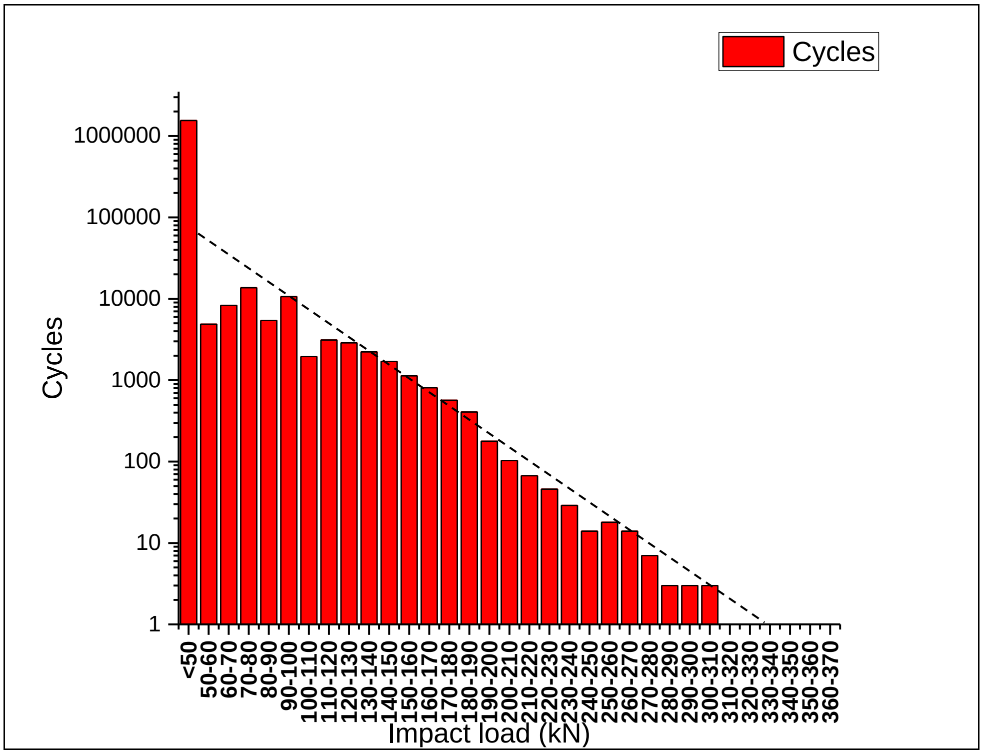

Figure 21. Field measurement of impact loads per year

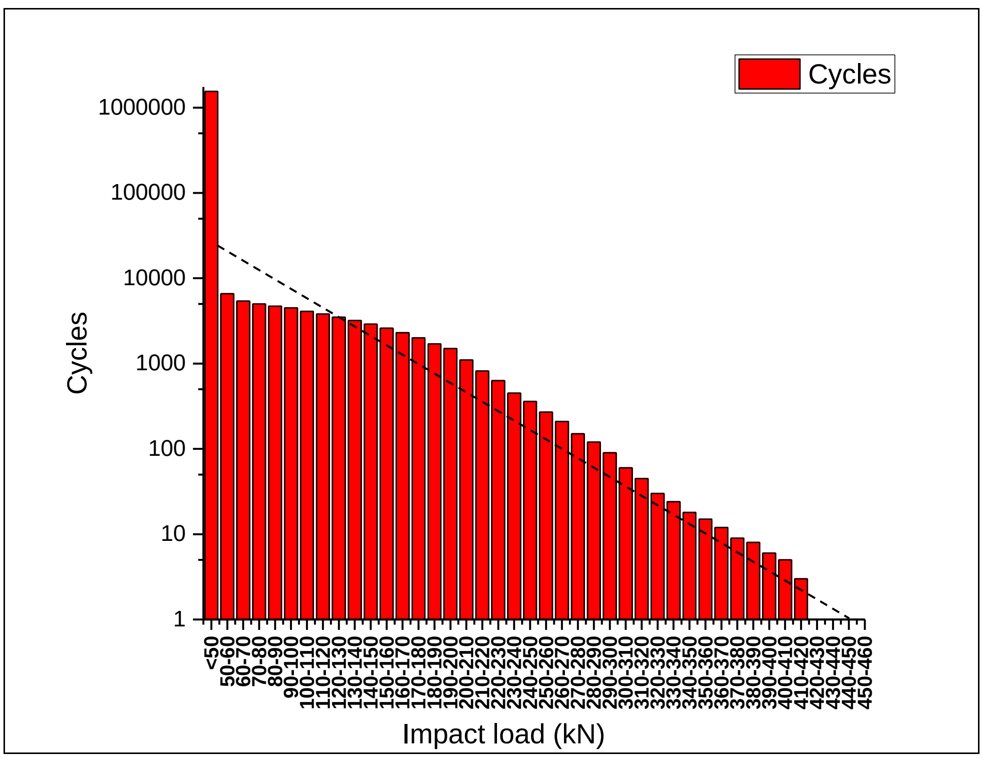

(a) Case 1

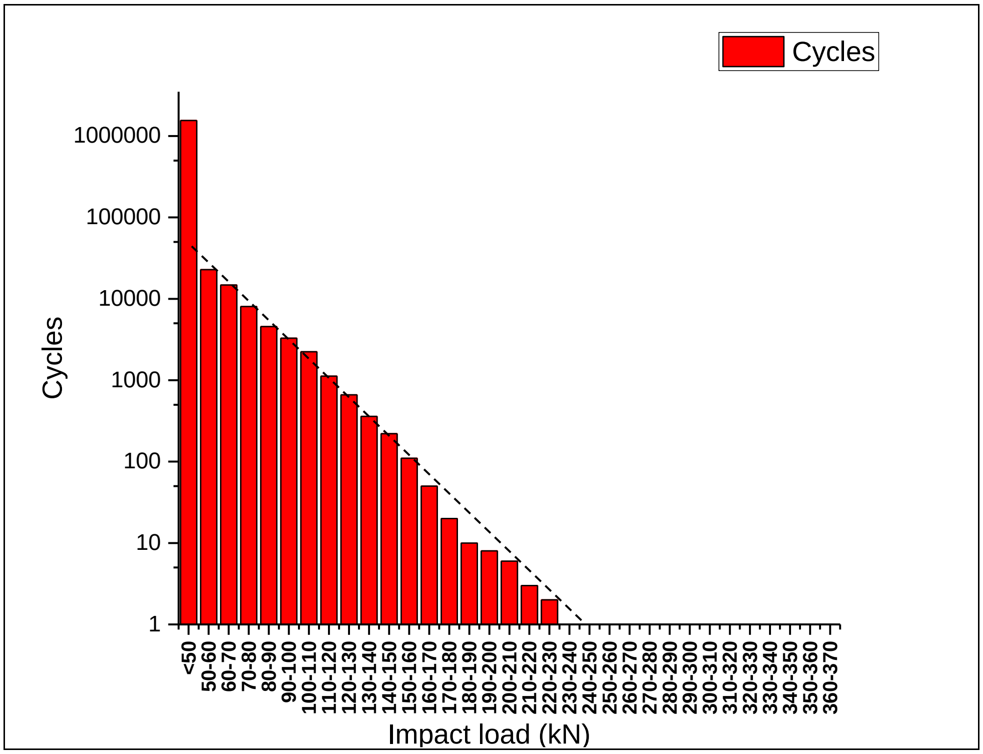

(b) Case 2

Figure 22. Case study of impact load distributions

	<50kN	**50-70kN**	**70-140kN**	**140-210kN**	**210kN<**	**Total cycles**
Case 1	1551481	12000	28800	14920	2484	1609711
Case 2	1551481	37600	20240	427	3	1609751
Field data	1551481	13179	39951	4963	138	1609712

Table 7. Impact load distributions

From **Table 10**, it can be seen that the total passing wheels per year for Case 1 and Case 2 are 1,609,711 and 1,609,751 respectively. They are very close to field measurement cycles (1,609,751 cycles) to ensure the distributions can be compared reasonable. Small impact loads (less than 50kN) for both Case 1 and Case 2 follow field data because small impact loads don't have significant effect on the fatigue life.

The total cycles (passing wheels) per year for Case 1, Case 2, and Field data are assumed following **Table 7** and keep the same every year, the damage index in each year can be determined. According to Miner's rule (Equation (1)), the fatigue life in years can be calculated. The outcome of the fatigue life with impact load distributions is shown in **Table 8**. There is not much difference in fatigue life between Case 1, Case 2, and the field measurement data as 96% of total cycles are small impact loads. From **Table 8**, it can be seen that the result of Case 1 is 14.28% less than field measurement data whereas the result of Case 2 is 8.51% higher than field measurement data. The results demonstrate greater large impact load occurrence can lead to the reduction of the service life of prestressed concrete sleepers. **Table 4** shows that the fatigue life is up to 4.19E+10 cycles under constant 55kN dynamic load which also indicates the large impact loads need to be controlled for increasing the service life of railway sleepers.

Impact load distribution	Life cycles	Years
Case 1	8.57E+08	32
Case 2	1.09E+09	37
Field data	1.00E+09	35

Table 8. Results of the fatigue life under different impact load distributions

7.3 Track stiffness

Track stiffness can influence the dynamic behaviour of trains, bearing capacity, track geometry, and service life of sleepers. This section discusses the effect of track stiffness on the fatigue life of prestressed concrete sleepers. In this section, the support condition is set as full contact pattern.

Previous research conducted by Martin, X et al (2010) [29] has investigated three levels of track stiffness (‘soft’, ‘normal’, and ‘stiff’) according to the static approach. The track properties are shown in **Table 9**. In their research, 100kN wheel load is applied. These track stiffness properties are input into the FE model to analyse the performance of the railway sleeper. The simulation results for ‘soft’, ‘normal’, and ‘stiff’ track are presented in **Table 10**.

	Track A: ‘soft’	Track B: ‘normal’	Track C: ‘stiff’
Stiffness of ballast/subgrade	10kN/mm	50kN/mm	100kN/mm
Rail displacement	3.16mm	1.28mm	0.58mm

Table 9. Track stiffness properties

Track type	Life cycles	Years
Soft	1.42E+09	42
Normal	1.08E+09	37
Stiff	9.63E+08	34

Table 10. Results of the fatigue life in different track stiffness

The results from **Table 13** indicate stiffer track have shorter life cycles. In comparison with these three types of tracks, the fatigue life of ‘soft’ track is 31.54% more than ‘normal’ track while that of ‘stiff’ track is 10.69% less than ‘normal’ track. The results show that high track stiffness increases dynamic load in the wheel-rail reaction and causes the reduction of life cycles. However, these results do not indicate stiffer tracks have worse performance than softer tracks because the parametric study only considers how track stiffness influences fatigue life. In actual track systems, relatively high track stiffness can provide sufficient track resistance and reduce deflections.

8 Conclusion

This paper aimed to develop a numerical model of prestressed concrete sleepers to effectively simulate the fatigue life and performance of railway sleepers under cyclic loads. The objective was to better understand mechanisms of fatigue problems of prestressed concrete sleepers by using an analytical model. To investigate fatigue life, the stress life method was chosen to develop a numerical model. This method is based on an empirical S-N curve and modified by a variety of factors. The theoretical assessment method is also presented in order to validate the numerical model. The model predictions for fatigue life successfully matched with theoretical results. Based on the obtained results of this study, the key findings are revealed as follows:

- Generally, dynamic loads significantly affect fatigue life. Fatigue life of prestressed concrete sleepers is inversely proportional to the magnitude of dynamic loads. This phenomenon indicates the high impact loads need to be controlled.
- Based on Stress Life method of fatigue analysis type, a numerical analysis of fatigue life has been conducted using FEM. The previous theoretical fatigue life assessment method is used for validation of the numerical fatigue life model.
- In numerical study, the S-N curve is used to define the alternating stress for calculating fatigue life. The equivalent alternating stress is determined by empirical stress theory.
- Statistical analysis of the fatigue loads from field measurement and their fatigue performance on the prestressed concrete sleeper.
- Development of reasonable numerical fatigue life model can be used on prestressed concrete sleepers. However, in practice, dynamic loads could be various due to different contact conditions. Therefore, the results of fatigue life only considering constant load are the limit to this research.
- On this point, it is important to note that rail/wheel irregularity needs to be considered in further study.

Parametric studies investigate the support conditions, impact load distribution, and track stiffness, which influence the fatigue life of railway sleeper. In general, the railway sleepers in conventional tracks are considered to have an ideal contact between the sleeper and ballast. However, in some situations problems could result in voids and pockets formed in the sleeper/ballast contact. Five support conditions are investigated. The stress distributions of the sleepers are analysed in order to determine the minimum fatigue life of each support patterns. In the support condition study, the positive moment at rail-seat is more critical than negative moment at midspan, which means the minimum fatigue life usually occurs at bottom rail-seat area. Central void support patterns do not influence the fatigue life much. In addition, regular tamping activities typically concentrate the ballast reaction below the rail seats, which is similar to central void support pattern. When the voids occur at the side of prestressed concrete sleepers, the life cycles reduce. With the side voids increasing, the life cycles decrease sharply. In actual life, the full support pattern is favorable for the rail seat sections but could be unfavorable for the centre section. Therefore, it is necessary to conduct track inspection to ensure well supported conditions. The results of impact load distributions indicate a greater proportion of high impact loads affect service life. Small proportions (1.1%) of high impact loads can cause 14% life cycle reduction. If the dynamic loads can be controlled no more than 70kN, the performance of railway sleepers is improved. The investigation of track stiffness reveals stiffer track can decrease the life cycles. High track stiffness results in increases of dynamic loads in wheel-rail reaction as well as sleepers, which causes the reduction of life cycles. It should be noted that the experimental programs are suggested to conduct in future research, which can be compared with theoretical and numerical results for more accurate prediction.

This article demonstrates a reliable approach for evaluating the fatigue life of prestressed concrete sleepers. The parametric study provides design flexibility and choices to engineers. The outcome of this paper will enhance the safety of the track component, and railway sleeper manufacturers could use the model to assess their product designs.

Acknowledgements

The authors are grateful to the Track Engineering and Operations for Future Uncertainties (TOFU) Lab, University of Birmingham for support throughout this study. The authors would like to thank the Commission for H2020-MSCA-RISE, Project No. 691135 “RISEN: Rail Infrastructure Systems

Engineering Network" (www.risen2rail.eu) [30]. Also, the first author wishes to thank the China Academy of Railway Science (CARS) for the collaborative project.

References

1. Esveld, C. and C. Esveld, *Modern railway track*. Vol. 385. 2001: MRT-productions Zaltbommel.
2. Steffens, D.M., *Identification and development of a model of railway track dynamic behaviour*. 2005, Queensland University of Technology.
3. Li, D., et al., *Parametric studies into creep and shrinkage characteristics in railway prestressed concrete sleepers.* Frontiers in Built Environment, 2020: p. 130.
4. Thun, H., *Assessment of fatigue resistance and strength in existing concrete structures*. 2006, Luleå tekniska universitet.
5. Ferdous, W. and A. Manalo, *Failures of mainline railway sleepers and suggested remedies–review of current practice.* Engineering Failure Analysis, 2014. **44**: p. 17-35.
6. Standard, A., *Railway track materials*, in *Part 14: Railway presterssed concrete sleepers*. 2003: Australian Standard AS1085.14.
7. Remennikov, A., M.H. Murray, and S. Kaewunruen, *Reliability-based conversion of a structural design code for railway prestressed concrete sleepers*. Proceedings of the Institution of Mechanical Engineers, Part F: Journal of Rail and Rapid Transit, 2012. **226**(2): p. 155-173.
8. Mosley, W.H., R. Hulse, and J.H. Bungey, *Reinforced concrete design: to Eurocode 2*. 2012: Macmillan International Higher Education.
9. You, R., et al., *Fatigue life assessment method for prestressed concrete sleepers.* Frontiers in built environment, 2017. **3**: p. 68.
10. Wakui, H. and H. Okuda, *A study on limit state design method for prestressed concrete sleepers.* Doboku Gakkai Ronbunshu, 1997. **1997**(557): p. 35-54.
11. Kaewunruen, S., *Experimental and numerical studies for evaluating dynamic behaviour of prestressed concrete sleepers subject to severe impact loading.* 2007.
12. Kaewunruen, S. and A. Remennikov, *On the residual energy toughness of prestressed concrete sleepers in railway track structures subjected to repeated impact loads.* 2013.
13. Kaewunruen, S., A.M. Remennikov, and M.H. Murray, *Introducing a new limit states design concept to railway concrete sleepers: an Australian experience.* Frontiers in Materials, 2014. **1**: p. 8.
14. Rantala, T., et al., *Fatigue loading tests of concrete railway sleepers*, in *High Tech Concrete: Where Technology and Engineering Meet*. 2018, Springer. p. 1445-1452.
15. Šimonová, H., et al. *Influence of the age and level of concrete fatigue on prestressed railway sleeper response: parametric study and experiment*. in *Advanced Materials Research*. 2014. Trans Tech Publ.
16. Maekawa, K., et al., *Three-dimensional fatigue simulation of RC slabs under traveling wheel-type loads.* Journal of Advanced Concrete Technology, 2006. **4**(3): p. 445-457.

17. Zhang, C., et al., *Fatigue Simulation Analysis of Carriageway Plates of Reinforced Concrete T-Shaped Girders.* Journal of Engineering Science & Technology Review, 2019. **12**(5).

18. You, R. and S. Kaewunruen, *Evaluation of remaining fatigue life of concrete sleeper based on field loading conditions.* Engineering Failure Analysis, 2019. **105**: p. 70-86.

19. du béton, F., *Precast Concrete Railway Track Systems: State-of-art Report*. 2006: International Federation for Structural Concrete (fib).

20. Standard, B., *Eurocode 2: Design of concrete structures*—. Part 1-1: General rules and rules for buildings, 2004: p. 230.

21. Ansys, *ANSYS® Academic Research Mechanical, Release 18.1*. 2018.

22. Browell, R. and A. Hancq, *Calculating and displaying fatigue results.* Ansys Inc, 2006. **2**.

23. Standardization, E.C.f., *EN 13230-2: Railway applications-track-concrete sleepers and bearers part 2: Prestressed monoblock sleepers.* 2009.

24. Li, D., S. Kaewunruen, and R. You, *Time-dependent behaviours of railway prestressed concrete sleepers in a track system.* Engineering Failure Analysis, 2021. **127**: p. 105500.

25. Parvez, A. and S.J. Foster, *Fatigue of steel-fibre-reinforced concrete prestressed railway sleepers.* Engineering Structures, 2017. **141**: p. 241-250.

26. Parvez, A. and S.J. Foster, *Fatigue behavior of steel-fiber-reinforced concrete beams.* Journal of Structural Engineering, 2015. **141**(4): p. 04014117.

27. Kaewunruen, S. and A. Remennikov, *Investigation of free vibrations of voided concrete sleepers in railway track system.* Proceedings of the Institution of Mechanical Engineers, Part F: Journal of Rail and Rapid Transit, 2007. **221**(4): p. 495-507.

28. Leong, J., *Development of a limit state design methodology for railway track*. 2007, Queensland University of Technology.

29. Li, M. and E. Berggren, *A study of the effect of global track stiffness and its variations on track performance: simulation and measurement.* Proceedings of the Institution of Mechanical Engineers, Part F: Journal of Rail and Rapid Transit, 2010. **224**(5): p. 375-382.

30. Kaewunruen, S., J.M. Sussman, and A. Matsumoto, *Grand challenges in transportation and transit systems.* Frontiers in built environment, 2016. **2**: p. 4.